Appl Phys B (2009) 95: 131–139
DOI 10.1007/s00340-009-3408-0

Applied Physics B
Lasers and Optics

Imaging performance and light emission efficiency of Lu_2SiO_5:Ce (LSO:Ce) powder scintillator under X-ray mammographic conditions

C. Michail · A. Toutountzis · S. David · N. Kalyvas · I. Valais · I. Kandarakis · G.S. Panayiotakis

Received: 7 June 2008 / Revised version: 30 December 2008 / Published online: 3 March 2009

Abstract The aim of the present study was to measure the imaging transfer characteristics and the luminescence efficiency (XLE) of a Lu_2SiO_5:Ce (LSO:Ce) powder scintillator for use in X-ray mammography detectors. An LSO:Ce powder scintillating screen, with a coating thickness of 25 mg/cm^2, was prepared in our laboratory. The imaging performance of the screen was assessed by experimental determination of the modulation transfer function (MTF) and the detective quantum efficiency (DQE) as well as single index image quality parameters such as noise equivalent pass band (Ne) and informational efficiency (n_1). A theoretical model, describing radiation and light transfer, was fitted to experimental MTF values in order to estimate optical properties of the scintillator. Screen irradiation was performed under exposure conditions employed in mammographic applications (27 kVp, 63 mAs). MTF was determined by the square wave response function (SWRF) method. Results showed that LSO:Ce exhibits high MTF and DQE values, which are comparable to those of the commercially used Gd_2O_2S:Tb. Considering our image quality parameters and luminescence efficiency results as well as the fast response of the LSO:Ce scintillator screen (40 ns), this material can be considered for use in X-ray mammographic detectors.

PACS 07.85.Fv · 42.30.Lr · 85.60.Gz

C. Michail · A. Toutountzis · S. David · N. Kalyvas · I. Valais · G.S. Panayiotakis (✉)
Department of Medical Physics, Medical School, University of Patras, 265 00 Patras, Greece
e-mail: panayiot@upatras.gr

N. Kalyvas · I. Valais · I. Kandarakis
Department of Medical Instruments Technology, Technological Educational Institution of Athens, Ag. Spyridonos, Aigaleo, 122 10 Athens, Greece

1 Introduction

Cerium (Ce^{3+})-doped scintillators are of particular interest for medical imaging applications due to their very fast response [1]. This is attributed to a 5d → 4f electronic transition in the Ce^{3+} ion [2, 3]. Lutetium oxyorthosilicate Lu_2SiO_5:Ce (LSO) is a scintillator with a number of advantages such as high light yield (26000 photons/MeV) and luminescence efficiency, high density (7.4 g/cm^3), fast decay time (40 ns), high effective atomic number (66) and excellent chemical stability [4–7]. Furthermore, LSO:Ce emits light in the blue region, which renders it compatible with a large number of optical sensors. In single-crystal form LSO:Ce has already been used in several non-imaging applications such as gamma-ray detection in nuclear physics, high-energy physics and environmental monitoring [4, 5]. LSO has also replaced $Bi_4Ge_3O_{12}$ (BGO) scintillators in some positron emission tomography (PET) scanners. However, to our knowledge LSO:Ce in powder form has not yet been employed in medical imaging applications, i.e. in medical radiographic detectors where powder scintillating screens are very often used. In previous works we have reported preliminary data on the performance of an LSO screen [8–10]. In the present study a systematic experimental and theoretical investigation of the light emission efficiency and the imaging performance of an LSO:Ce powder scintillating screen was performed under X-ray mammography conditions. Various parameters, such as the X-ray luminescence efficiency (XLE), the detector quantum gain (DQG) and spatial frequency-dependent imaging parameters, such as the modulation transfer function (MTF), the noise transfer function (NTF) and the detective quantum efficiency (DQE), were assessed. In addition, single index image quality parameters such as the noise equivalent pass

band (Ne) and the informational efficiency (η_I) were also evaluated.

2 Materials and methods

2.1 Theoretical interpretation

2.1.1 Output signal and signal transfer efficiency

The light emitted (output signal) by an irradiated scintillating screen may be expressed by either the emitted light energy fluence Ψ_Λ (light energy per unit of area) or the emitted light photon fluence Φ_Λ (light photons per unit of area) [11–14]:

$$\Psi_\Lambda(E_0, w) = \int_0^{E_0} \Psi_0(E)\eta_\varepsilon(E, w)\eta_C g_\Lambda(E, \sigma, \tau, w)\,\mathrm{d}E, \tag{1a}$$

$$\Phi_\Lambda(E_0, w) = \int_0^{E_0} \Phi_0(E)\eta_Q(E, w)m_\lambda g_\Lambda(E, \sigma, \tau, w)\,\mathrm{d}E, \tag{1b}$$

where $\Psi_0(E)$ denotes the incident X-ray energy fluence spectral distribution (energy fluence per energy interval) and $\Phi_0(E)$ denotes the incident X-ray photon fluence spectral distribution (photon fluence per energy interval). E is the X-ray photon energy and E_0 is the maximum energy of the X-ray spectrum. $\eta_\varepsilon(E, w)$ is the energy absorption efficiency (EAE), which is the fraction of incident X-ray energy absorbed locally at the points of X-rays' interaction within the scintillator. $\eta_Q(E, w)$ is the quantum detection efficiency (QDE), being the fraction of the total number of incident X-ray quanta interacting in the scintillator. η_C is the intrinsic X-ray to light conversion efficiency expressing the fraction of absorbed X-ray energy converted into light energy within the screen material [11–14]. m_λ is the intrinsic quantum conversion gain, i.e. the number of light quanta generated within the scintillator per absorbed X-ray of energy E. g_Λ is the light transmission efficiency [11–14], which represents the fraction of light escaping the scintillator. σ and τ are optical attenuation coefficients [11–13] representing the reciprocal light diffusion length and the inverse relaxation length, respectively [11–14].

In the present work the light energy fluence and the light photon fluence were modeled according to previously published theoretical models [12, 13]. If (1a) and (1b) are divided by the corresponding X-ray energy and X-ray photon fluence, two parameters expressing the light emission efficiency of scintillating screens may be defined. These two parameters are (a) the X-ray luminescence efficiency XLE (η_ψ), defined as the ratio of the emitted light energy fluence over the incident X-ray energy fluence Ψ_0 : ($\eta_\Psi = \Psi_\Lambda/\Psi_0$) and (b) the quantum detector gain QDG defined as the ratio of the emitted light photon fluence over the incident X-ray photon fluence: ($\eta_G = \Phi_\Lambda/\Phi_0$) [12–14].

Relations (1a) and (1b) may be expressed in the spatial frequency domain. Within this framework the detector quantum gain may be expressed by a gain transfer function (GTF), defined as follows:

$$\mathrm{GTF}(E_0, \nu, w) = \Phi_\Lambda(E_0, \nu, w)/\Phi_0, \tag{2}$$

where ν denotes spatial frequency and $\Phi_\Lambda(E_0, \nu, w)$ is the spatial frequency-dependent emitted light photon fluence.

To express strictly the imaging properties of a scintillating screen, independently of the emission efficiency, they are often expressed through the modulation transfer function (MTF) [12–17] defined by the spatial frequency-dependent light photon fluence normalized to zero frequency, as follows:

$$\mathrm{MTF}(E_0, \nu, w) = \Phi_\Lambda(E_0, \nu, w)/\Phi_\Lambda(E_0, \nu = 0, w). \tag{3}$$

If $\Phi_\Lambda(E_0, \nu, w) = \mathrm{MTF}(E_0, \nu, w) \cdot \Phi_\Lambda(E_0)$ is divided by the incident X-ray photon flux Φ_0 the gain transfer function may be expressed as follows:

$$\mathrm{GTF}(\nu, w) = \mathrm{MTF}(\nu, w)\eta_G, \tag{4}$$

where η_G is the quantum detector gain. In medical imaging, where fluorescent screens are used in combination with optical detectors (films, photocathodes, photodiodes), the spectral matching between the emitted phosphor light and the optical detector sensitivity must be taken into account. This is because the degree of spectral matching affects the amount of light utilized to form the final image. Thus, (4) is reduced by a factor a_S, expressing the fraction of emitted light that can be detected by the optical detector, which exhibits a specific spectral distribution of sensitivity. a_S can be calculated by (5):

$$\alpha_S = \frac{\int S_P(\lambda)S_D(\lambda)\,\mathrm{d}\lambda}{\int S_P(\lambda)\,\mathrm{d}\lambda}, \tag{5}$$

where $S_P(\lambda)$ is the spectrum of the light emitted by the phosphor and $S_D(\lambda)$ is the spectral sensitivity of the optical detector coupled to the phosphor [21]. Spectral matching factor values for LSO:Ce are shown in Table 1 [13, 18]. By taking into account a_S, we may define the effective gain transfer function as follows:

$$\mathrm{eGTF}(\nu, w) = \mathrm{DQG} \cdot \mathrm{MTF}(\nu, w) \cdot \alpha_S. \tag{6}$$

2.1.2 Signal to noise ratio and detective quantum efficiency

The output noise of a scintillating screen is expressed by the variance in the emitted light photon fluence over the screen

Table 1 Spectral matching factors of the LSO:Ce screen

Optical detector	Lu_2SiO_5:Ce
GaAs photocathode	0.92
a-Si	0.62
AmorSi	0.58
MAMORAY	0.87
E/S 20	0.96
AgfaGS	0.96
KodakGR	0.96
FujiUM	0.90
aSi108H	0.58
CCD S100AB SITe®	0.87
PSPMT Hamamatsu 8500	0.85

emitting area. In the spatial frequency domain noise is expressed by the noise power spectrum (NPS) [14–16, 19]. The NPS associated with the emitted optical photons generated at depth w and escaping to the output may be written as follows [19]:

$$\mathrm{NPS}(\nu, w) = \int \Phi_\Lambda m_\lambda g_\lambda(w, \sigma, \tau)\mathrm{MTF}^2(\nu, w)\,\mathrm{d}E + \Phi_\Lambda(E_0). \tag{7}$$

The noise transfer function (NTF) is expressed as

$$\mathrm{NTF}(E_0, \nu, w) = \left[\frac{\mathrm{NPS}(E_0, \nu, w)}{\mathrm{NPS}(E_0, 0, w)}\right]^{1/2}, \tag{8}$$

where $\mathrm{NPS}(E_0, u, w)$ is the spatial frequency-dependent noise power spectrum and $\mathrm{NPS}(E_0, 0, w)$ is the zero-frequency noise power spectrum. The square of the modulation transfer function over the noise transfer function, $R_c(v)$, is a measure of the different behavior in the transfer efficiency of the signal and the noise as they pass through the screen.

The detective quantum efficiency of a scintillating screen has been defined by the relation $\mathrm{DQE} = \mathrm{SNR}^2_{\mathrm{out}}/\mathrm{SNR}^2_{\mathrm{in}}$ [15]. In this relation, $\mathrm{SNR}_{\mathrm{out}}$ and $\mathrm{SNR}_{\mathrm{in}}$ are the output and input signal to noise ratios, respectively. In the spatial frequency domain DQE may be written as follows:

$$\mathrm{DQE}(\nu, w) = \frac{(\Phi_\Lambda(E_0, w)\mathrm{MTF}(E_0, \nu, w))^2}{\mathrm{NPS}(E_0, \nu, w)\mathrm{SNR}^2_{\mathrm{in}}}. \tag{9}$$

The input signal to noise ratio has been previously expressed, for an X-ray imaging detector, by (10)

$$\mathrm{SNR}^2_{\mathrm{in}} = \left(\int_0^{E_0} \Phi_0(E)E\,\mathrm{d}E\right)^2 \Big/ \int_0^{E_0} \Phi_0(E)E^2\,\mathrm{d}E, \tag{10}$$

where the numerator is equal to the square of the first statistical moment of the distribution of X-ray photons. This distribution is expressed by the X-ray spectral distribution of $\Phi_0(E)$ [15]. This is also equal to the square of the total incident X-ray energy fluence (input signal). The denominator is equal to the second moment of the aforementioned distribution. This second moment has been considered to express the input quantum noise.

2.2 Experiments and calculations

LSO:Ce was purchased in powder form (Phosphor Technology Ltd, England, code: ZBK58/N-S1) with mean grain size of approximately 8 μm and a density of 7.4 g/cm^3. Particle size and morphology parameters of the LSO:Ce powder phosphor were verified via scanning electron microscope (SEM) micrographs using a Jeol JSM 5310 scanning electron microscope collaborating with the INCA software. Gold was used to obtain a figure from a site of interest of the LSO:Ce specimen. For the elementary particle analysis a carbon thread evaporation process was used. Carbon was flash evaporated under vacuum conditions to produce a film suited for the LSO:Ce SEM specimen in a BAL-TEC CED 030 carbon evaporator ($\sim 10^{-2}$ mbar). The phosphor was used in the form of a thin layer (test screen) to simulate the intensifying screens employed in X-ray mammography. For the purposes of the present study, a 25 mg/cm^2 thick scintillating screen was prepared by sedimentation of LSO:Ce powder on a fused-silica substrate (Spectrosil B). During the sedimentation process, sodium orthosilicate (Na_2SiO_3) was used as binding material between the powder grains [19, 22].

Experiments were performed on a General Electric Senographe DMR Plus X-ray mammographic unit with molybdenum anode target and molybdenum filter. For the determination of the XLE, X-ray tube voltages ranging from 22 to 40 kVp with molybdenum anode target and molybdenum filter were used. The filter changed automatically from molybdenum (Mo) to rhodium (Rh) and aluminum (Al) as tube voltage increased, at 35 and 42 kVp, respectively. Tube voltage and incident exposure rate were checked using a Victoreen dosimeter (model 4000 M+).

The X-ray luminescence efficiency η_ψ was determined by performing X-ray exposure and emitted light energy flux measurements. Ψ_Λ measurements were performed using an experimental setup comprising a light-integration sphere (Oriel 70451) coupled to a photomultiplier (EMI 9798B) connected to a Cary 401 vibrating reed electrometer [23]. For the calculation of XLE, the X-ray energy flux, Ψ_0 in (1a), was determined by converting X-ray exposure data X [24] as follows: $\Psi_0 = X\hat{\Psi}$, where $\hat{\Psi}$ is a function defined as the X-ray energy flux per exposure rate, which

may be estimated as follows:

$$\hat{\Psi} = \int \Psi_0(E)\,\mathrm{d}E \Big/ \left(\int \Psi_0(E)[X/\Psi_0(E)]\,\mathrm{d}E \right), \tag{11}$$

where

$$X/\Psi_0(E) = \left(\mu_{\mathrm{en}}(E)/\rho\right)_{\mathrm{air}} \cdot (W_{\mathrm{A}}/e)^{-1} \tag{12}$$

is the factor converting energy flux into exposure rate, $(\mu_{\mathrm{en}}/\rho)_{\mathrm{air}}$ is the X-ray mass energy absorption coefficient of air at energy E and W_{A}/e is the average energy per unit of charge required to produce an electron–ion pair in air. The values of W_{A}/e and $(\mu_{\mathrm{en}}/\rho)_{\mathrm{air}}$ were obtained from the literature [25].

Detector quantum optical gain (DQG) was determined according to the ratio Φ_Λ/Φ_X. The emitted light photon fluence may be expressed in terms of experimentally measurable quantities (absolute efficiency, exposure, mean light wavelength) by using (13):

$$\Phi_\Lambda = \Psi_\Lambda / hc\bar{\lambda}^{-1}, \tag{13}$$

where the numerator is equal to the light energy fluence and the denominator is equal to the mean energy E_λ of the emitted light photons ($E_\lambda = hc/\bar{\lambda}$), $\bar{\lambda}$ being the mean light wavelength determined from emission spectra measurements [8] as follows:

$$hc\bar{\lambda}^{-1} = hc\left\{ \int \phi_\Lambda(\lambda)\lambda\,\mathrm{d}\lambda \Big/ \int \phi_\Lambda(\lambda)\,\mathrm{d}\lambda \right\}^{-1}, \tag{14}$$

where $\phi_\Lambda(\lambda)$ is the measured scintillator's emission spectrum [8]. Φ_X was determined by using (11) and (12), replacing Ψ_0 by Φ_0 and dividing (12) by the X-ray energy [23].

MTF was experimentally determined by the square wave response function (SWRF) method [26]. A Nuclear Associates resolution test pattern (type 53, Nuclear Associates) containing Pb lines of various widths corresponding to various spatial frequencies (from 0.25 to 10 lp mm^{-1}) was used to obtain pattern images. The screen was brought in close contact with a radiographic film (Kodak T-Mat) enclosed in a light-tight cassette. The film–screen combination was irradiated by X-rays on the mammographic unit. The exposure conditions employed for the MTF measurements were 27 kVp and 63 mAs. Two modes for the measurement of the MTF were followed: (1) reflection mode, where light emitted by the irradiated screen side was measured (the film was placed behind the test pattern and in front of the screen); (2) transmission mode, where the non-irradiated screen side's light was measured (the film was placed behind the screen). Reflection mode represents the conventional mammography intensifying screens and the rear screens of an ordinary radiographic cassette. Transmission mode simulates the detector configuration in all the other X-ray-imaging modalities.

After irradiation, films were developed in an Agfa Scopix LR 5200 film processor, operated at 36°C and at 90-s processing time. Pattern images, obtained on the films, were digitized in an Agfa Duoscan scanner with scanning parameters 1000 dpi and 8 bits. Prior to digitization it was verified that the film optical density values were within the linear part of the characteristic curve between exposure and film density (Hurter & Driffield or H&D curve). MTFs were finally calculated from the digitized image optical density variations (digital SWRFs). The latter were obtained across directions vertical with respect to the test-pattern lines, employing Coltman's formula [26, 27], which gives the MTF as a function of SWRF. The MTF data, obtained in this way, were corrected by dividing by the MTF of the scanner and the MTF of the film, both measured in a previous study [9]. The gain transfer function was estimated from MTF and QDG values by using (4).

The noise transfer function (NTF) was obtained through the noise power spectrum (NPS). The NPS was estimated through the measurement of Ψ_Λ according to a method described in [28]. The noise transfer function is then obtained according to (8).

The detective quantum efficiency DQE was estimated by MTF, NTF, Φ_{X} and Ψ_Λ . Finally, the DQE may be expressed in terms of quantities that can be experimentally determined:

$$\mathrm{DQE}(\nu, w) = \frac{[\Psi_\Lambda]^2}{(hc/\bar{\lambda})^2} \frac{1}{\mathrm{SNR}_{\mathrm{in}}^2 \cdot \mathrm{NPS}(E_0, 0, w)} [R_{\mathrm{c}}(\nu)]. \tag{15}$$

Since the spatial frequency sampling steps of MTF and NPS are generally not the same, NPS was linearly interpolated at the frequency sampling points of MTF and then DQE was calculated at these points. Detective quantum efficiency was calculated for both reflection and transmission modes.

Beyond the spatial frequency-dependent parameters described before, image quality can be expressed by single index parameters. The following two parameters, called noise equivalent pass band (Ne) and informational efficiency (η_I), provide such indices which may be the value at zero spatial frequency or the integral over the useful range of exposures. Calculation of these parameters was based on the experimentally measured values of the modulation transfer function. The noise equivalent pass band, expressing image sharpness by a single number, has been defined [29] by (16):

$$\mathrm{Ne} = 2\int_0^\infty \mathrm{MTF}^2(\nu, w)\,\mathrm{d}\nu. \tag{16}$$

Relation (16) describes Ne as a quantity proportional to the area under the curve of MTF squared.

Informational efficiency (η_{I}) compares the imaging performance of real imaging systems to the performance of

perfect (ideal) systems [14] by a single index. The informational efficiency has been defined [14] as

$$\eta_1(E, w) = \frac{\mathrm{DQE}(0)\mathrm{Re}(E, w)}{\int_0^\infty \nu \, \mathrm{d}\nu}, \tag{17}$$

where Re corresponds to an ideal imaging system.

3 Results and discussion

Qualitatively the particles of LSO:Ce phosphor have a mean grain size of 8 μm (obtained from Phosphor Technology Ltd, England, code: ZBK58/N-S1 data sheet). Figure 2 shows the grain-size distribution of the LSO:Ce phosphor, estimated from scanning electron microscope (SEM) images. The mean grain size was found to be 8.63 μm. A fragment image of LSO:Ce powder phosphor is presented in Fig. 1. It was shown by energy dispersive X-ray (EDX) analysis that the powder is really Lu_2SiO_5:Ce with no admixtures.

The X-ray characteristic curve (signal versus exposure) is plotted in Fig. 3 and shows a linear dependence between output signal and exposure rate in the 4.8–114 mR/s range. The linear no-threshold fit gave a reduced R^2 of 0.9928, which is very close to the most likely reduced R^2 value and indicates a satisfactory fit.

Figure 4 shows the X-ray luminescence efficiency for the 25 mg/cm^2 phosphor screen for various tube voltages. To provide a more detailed insight into the conversion and emission properties of LSO:Ce scintillator, a comparison between the X-ray luminescence efficiency and the absorbed X-ray to emitted light conversion efficiency (ECE) is plotted in the same figure. ECE expresses the fraction of ab-

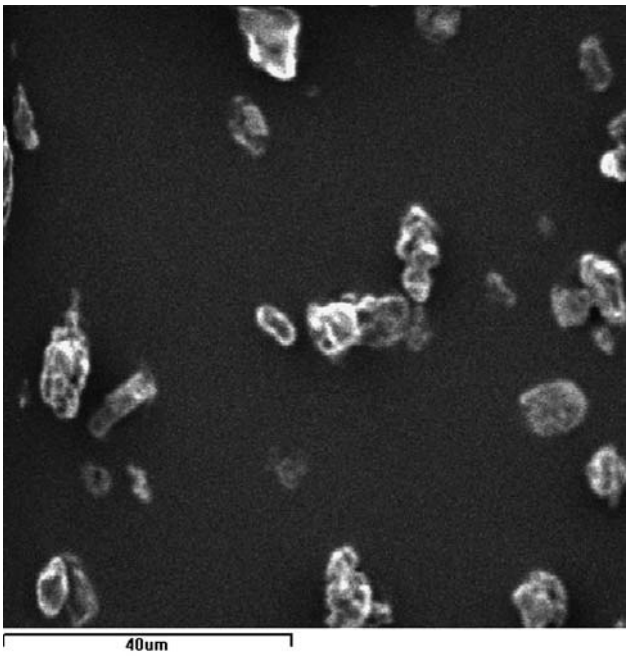

Fig. 1 Scanning electron microscope (SEM) image from a site of interest of the LSO:Ce phosphor

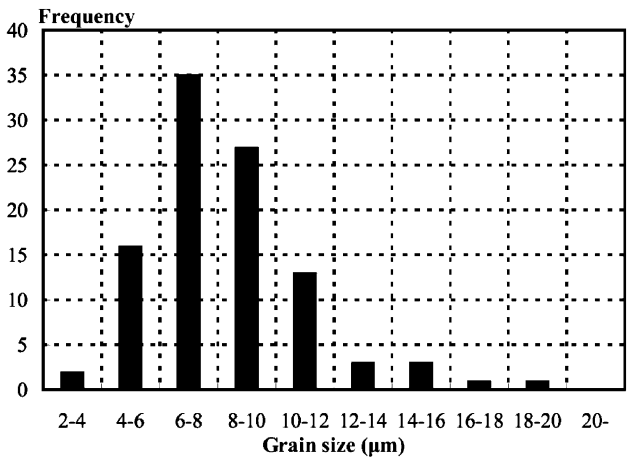

Fig. 2 Grain-size distribution obtained from SEM images of the LSO:Ce phosphor

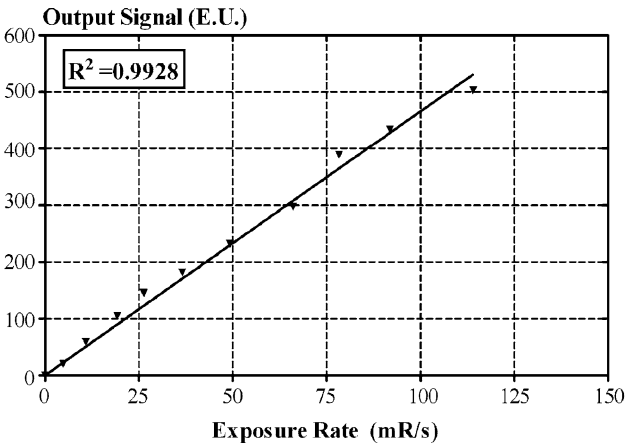

Fig. 3 Characteristic curve of the LSO:Ce phosphor screen in the mammographic range of exposures. The *triangles* are the measured values and the *solid line* is a linear no-threshold fit to the data

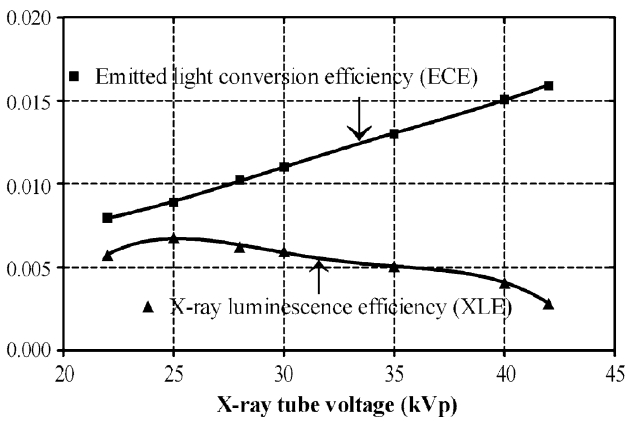

Fig. 4 Variation of XLE and ECE with X-ray tube voltage

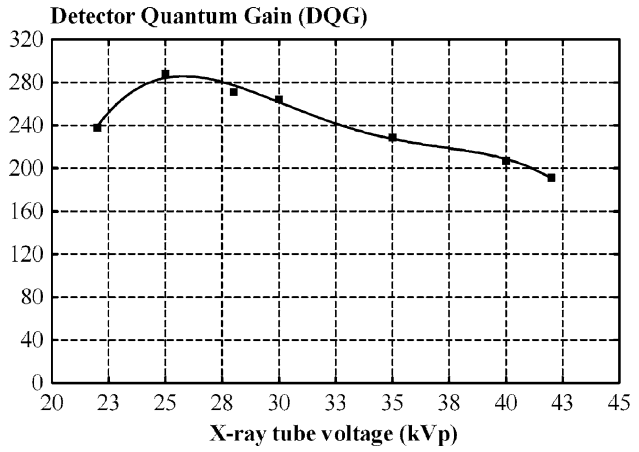

Fig. 5 DQG of the LSO:Ce phosphor screen at various mammographic X-ray energies

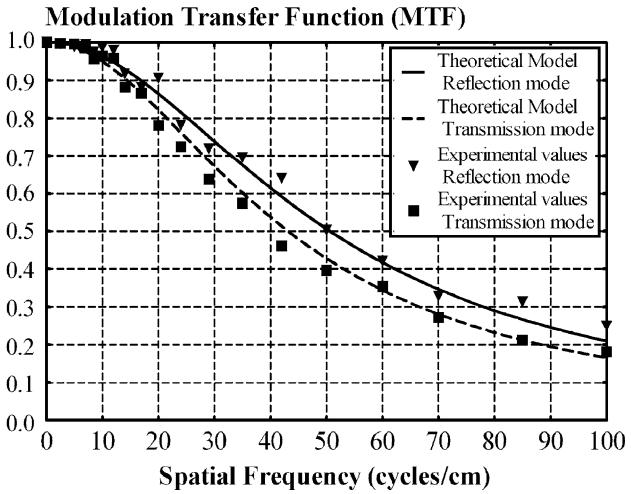

Fig. 6 Comparison of the experimentally determined MTFs of the LSO:Ce powder phosphor screen with the MTF produced by the theoretical model in reflection and transmission modes

sorbed X-ray energy that is converted into light emitted by the screen surface. ECE was calculated by the product $\mathrm{ECE} = n_c \cdot G_A(E, \sigma, \tau, \rho)$ [23]. A first point to make is that, neglecting the XLE values in the 22 to 25 kVp X-ray tube voltage range, a tendency of the XLE to decrease with increasing tube voltage is clearly shown. The main reason governing this behavior should be attributed to the energy absorption properties of the phosphor [8]. However, the shape of the XLE curves should be additionally affected by the light transmission through the screen. As X-rays penetrate deeper in the phosphor mass, at higher voltages, light photons are created closer to the screen output. Light is thus more easily transmitted through the phosphor grains. On the other hand, low-energy X-rays do not penetrate deeply within the scintillator mass. Hence, light photons, which are mainly created very close to the input screen surface, are forced to travel long trajectories to escape the rear surface of the screen. This increases light attenuation (self absorption) within the scintillator mass. This effect may explain the decreased XLE values obtained at 22 kVp. It is of interest to note that XLE (i.e. emitted light energy per incident X-ray energy) and ECE (i.e. emitted light energy per absorbed X-ray energy) have clearly different shapes. The ECE curve continuously increases with increasing tube voltage, i.e. from 0.0079 at 22 kVp to 0.0159 at 42 kVp while XLE has a peak value at 25 kVp. This is because the shape of the ECE curve is determined solely by light attenuation effects while the XLE is affected by both X-ray absorption and light attenuation. Light attenuation is of lower importance at high voltages since X-ray penetration is deeper and light has to travel shorter distances through the remaining screen mass. This is favorable for light emission in transmission mode and explains the increased slope of the ECE curve.

The detector quantum gain of the LSO:Ce screen is shown in Fig. 5. The curve shows a similar shape to the XLE curve. In the present case the shape of the DQG curve may be explained by considering the combined effects of energy losses, expressed by XLE, and of signal amplification, expressed by the ratio E_X/E_λ (X-ray over light photon mean energy, see (10)) which changes rather slowly with X-ray energy. This is because in the mammography range the mean energy of X-ray photons shows a slight increase with tube voltage. This is due to the strong influence of the Mo spectral lines at 17.5 and 19.5 keV in the mean X-ray photon energy. DQC values found in this study for the 25 mg/cm^2 LSO:Ce phosphor screen at 20 keV are comparable to the corresponding values of the widely used 31 mg/cm^2 Gd_2O_2S:Tb (GDOS:Tb) Kodak Min-R screen published by others [20].

Figure 6 shows experimentally obtained MTF curves of the LSO:Ce screen measured at 27 kVp in reflection and transmission modes compared with the theoretical model predictions. Points represent experimental data while the line represents the theoretical model fitted curve to the experimental data. The values of the inverse relaxation length and the light attenuation coefficient estimated by this fitting were $\tau = 2333.3$ cm^2 g^{-1} and $\sigma = 70$ cm^2 g^{-1}, respectively. The value of η_C was found to be 0.08 according to a previous publication [8]. Experimental MTF results were found higher in reflection than in transmission mode. In reflection mode, the theoretical model simulation shows better agreement with the experimental MTF values than in transmission. In transmission mode a slight overestimation was found in the low and medium frequency ranges.

MTFs calculated by the theoretical model are shown in Fig. 7. In this figure the MTF curves of seven LSO:Ce screens with coating thicknesses of 19, 25, 31, 45, 57, 63 and 80 mg/cm^2 are shown. Calculations were performed by using (3) and the optical values determined by the fitting. Curves were calculated by using a Mo X-ray spectrum to simulate mammographic conditions at 27 kVp. It

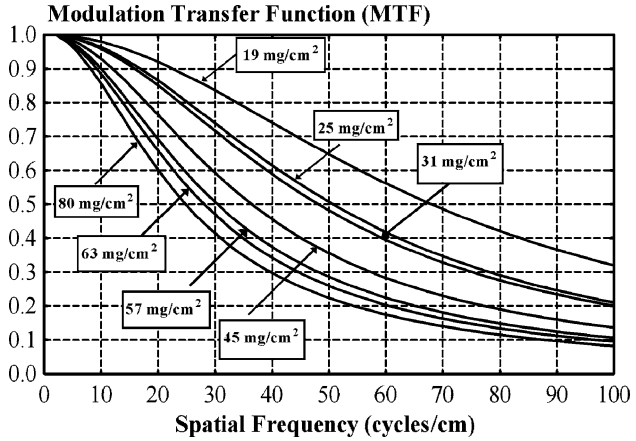

Fig. 7 MTFs of the LSO:Ce powder phosphor for various screen coating thicknesses obtained by the theoretical model in reflection mode

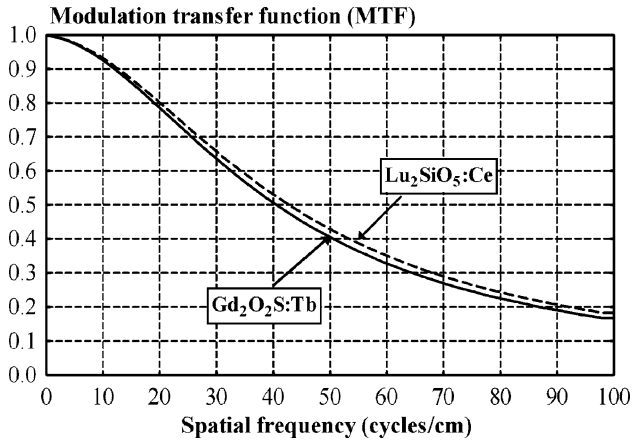

Fig. 8 Calculated MTF comparison between LSO:Ce and GDOS:Tb, in mammographic conditions for 35 mg/cm^2 screens at 27 kVp

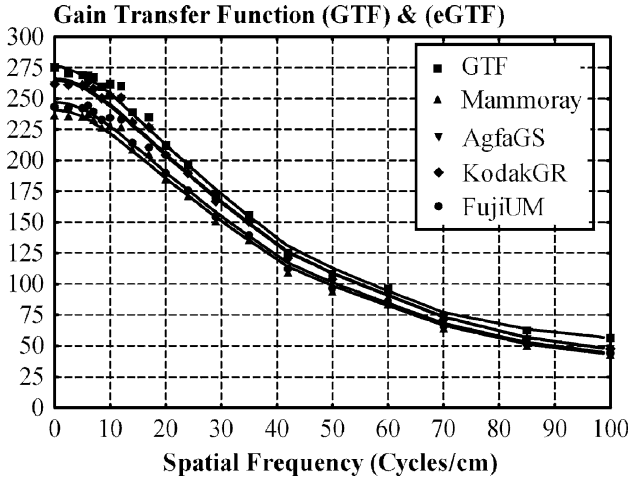

Fig. 9 Variation of the GTF and eGTF with spatial frequency for the LSO:Ce phosphor screen combined with the various film types

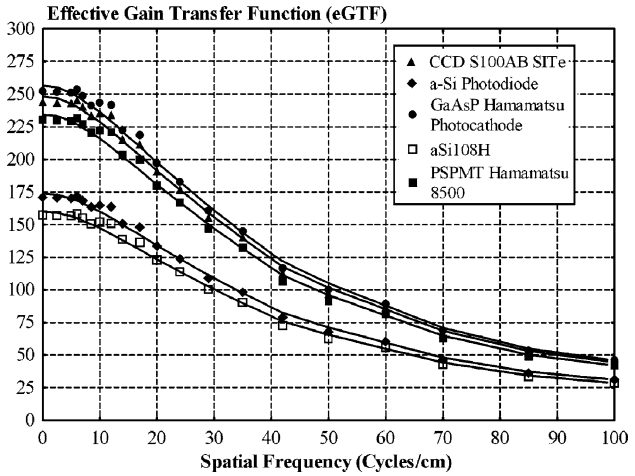

Fig. 10 Variation of the eGTF with spatial frequency for the LSO:Ce phosphor screen combined with the various digital detectors

can be observed that the MTF curves do not change significantly for screens thicker than 63 mg/cm^2. As the coating thickness increases, MTF decreases. This may be physically explained by the increased light spread into the phosphor mass. Figure 8 shows a comparison between theoretically calculated MTFs of LSO:Ce and the commercially used GDOS:Tb phosphor, using a 27 kVp Mo spectrum with 35 mg/cm^2 screen thickness for mammographic conditions. These findings indicate that the spatial resolution and sharpness of LSO:Ce may be better than GDOS:Tb. This may be attributed to deviations in light output, i.e. the blue light emitted by the LSO:Ce screen shows higher optical attenuation within the phosphor mass. Thus, laterally directed photons (traveling longer distances to reach the screen surface) are strongly attenuated, resulting in reduced light spreading.

Figures 9 and 10 show the variation of GTF and eGTF with spatial frequency for the LSO:Ce phosphor screen measured at 27 kVp. The difference between this curve and the corresponding MTF curves is due to the influence of X-ray absorption and optical emission on GTF, which are more apparent at lower frequencies. As frequency increases, the influence of MTF on GTF is more significant than the corresponding influence of detector quantum gain causing a further decrease in the GTF. Figure 9 shows the effective GTF of the LSO:Ce screen with various films. The best film–screen combination was obtained for the Kodak GR film while the best combination with electronic detectors was obtained for the GaAsP Hamamatsu photocathode. However, it is of importance to note that very high eGTF values are also obtained with the CCD detector, which is often used in digital mammography detectors [30]. In addition, adequate eGTF values were obtained with the a-Si detector, used in modern flat-panel imagers.

Figure 11 shows the noise transfer function (NTF) of the LSO:Ce phosphor screen. NTF decreases with spatial frequency, although at a slower rate than MTF. This is because noise is transferred more efficiently than signal in the higher

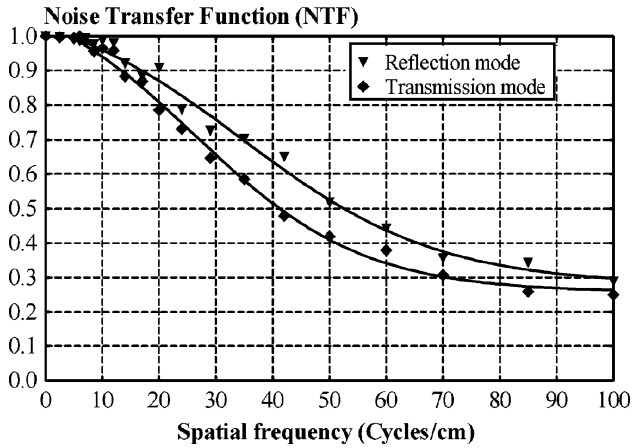

Fig. 11 NTF of the LSO:Ce screen in reflection and transmission modes

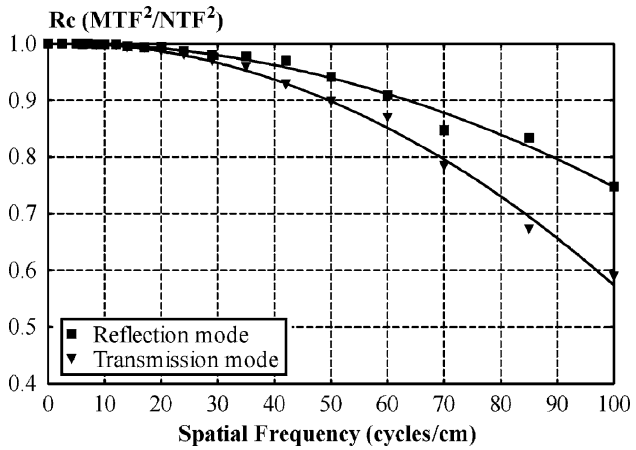

Fig. 12 Square of the MTF over the NTF ratio

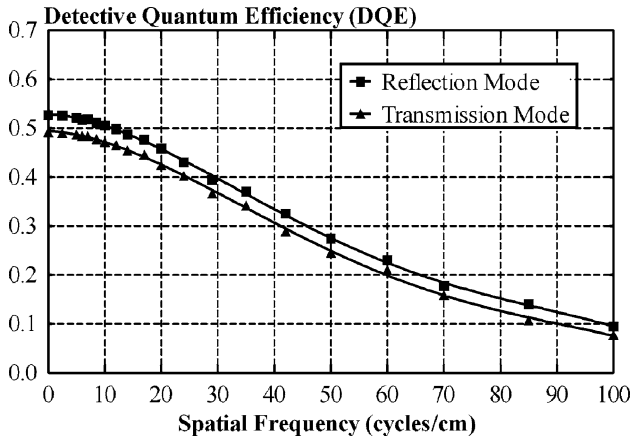

Fig. 13 DQE of the 25 mg/cm^2 LSO:Ce screen at 27 kVp, 63 mAs

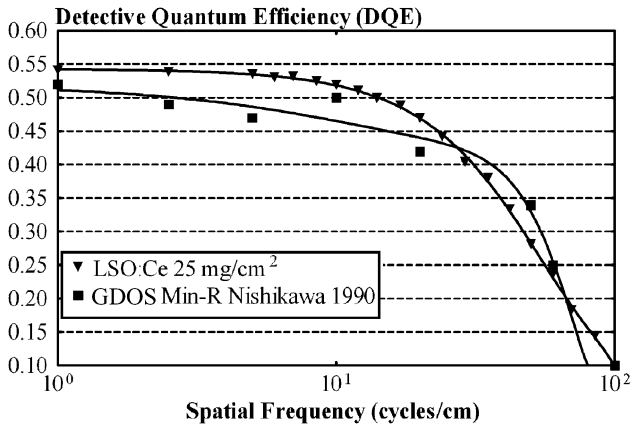

Fig. 14 DQE comparison between LSO:Ce and GDOS:Tb

spatial frequencies, as has been shown in a previous publication [20].

Figure 12 shows $R_c(\nu)$. The ratio $\mathrm{MTF}^2(\nu)/\mathrm{NTF}^2(\nu)$ decreases gradually with spatial frequency due to the high MTF values and the gradual fall off of the NPS curve, showing that noise passes more easily than the useful signal through the screen.

Figure 13 shows the detective quantum efficiency DQE of the 25 mg/cm^2 LSO:Ce phosphor screen in reflection and transmission modes. Reflection-mode DQE is superior than transmission mode. Zero-frequency DQEs for both modes are 0.54, which, however, are lower than the corresponding detection efficiency, which is 0.73. DQE at zero and low spatial frequencies is limited by the X-ray absorption efficiency of the detector material. DQE can never exceed the absorption efficiency (QDE) since DQE(0) $\leq$ QDE. DQE decreases with increasing frequency, being principally affected by $R_c(\nu)$. These DQE findings of our LSO:Ce screen are compared to published data for GDOS:Tb in Fig. 14 (Kodak Min-R screen at 30 kVp, 31.7 mg/cm^2) [20]. DQE of LSO:Ce is better at lower and higher spatial frequencies.

Finally, the calculated values for the noise equivalent pass band and informational efficiency ((16) and (17)) of LSO:Ce were found to be 25.87 and 0.1843, respectively. These values are higher than those of the GDOS:Tb screen (23.42 and 0.1381, respectively).

4 Summary and conclusions

In the present study, an LSO:Ce powder scintillator screen of 25 mg/cm^2 coating thickness was prepared and examined under X-ray mammography conditions. The spatial frequency-dependent (MTF and DQE) as well as the single index image quality parameters examined in this study reveal a promising material which can be an alternative to the established phosphors used in mammographic detectors. An LSO:Ce screen was found to have a slightly higher MTF than the commercially used Kodak Min-R screen. The superiority of reflection over transmission mode MTF values indicates the better resolution properties of conventional

(reflection) over digital (transmission) mammography detectors for identical phosphor material and equal phosphor thickness. Reflection-mode DQE is also superior to transmission mode. Detective quantum efficiency of LSO:Ce appeared to be better than the commercially used Kodak Min-R screen at lower and higher spatial frequencies. Furthermore, informational efficiency, as well as the noise equivalent pass band of the LSO:Ce screen, have greater values than those of GDOS:Tb. Taking into account that LSO:Ce has (i) high absorption efficiency at low X-ray energies, (ii) adequate image-quality properties (MTF and DQE) and (iii) very fast response, it could be considered for applications in both digital and conventional X-ray mammography detectors.

Acknowledgements The above work is funded by the Greek State Scholarships Foundation (I.K.Y.). The authors would like to thank Dr. Alexis Stefanis, from the Department of Conservation of Antiquities and Works of Art, TEI of Athens, for the SEM measurements.

References

1. J.A. Rowlands, J. Yorkston, in *Handbook of Medical Imaging*. Physics and Psychophysics, vol. 1 (SPIE, Bellingham, 2000)
2. C.W.E. van Eijk, Phys. Med. Biol. **47**, 85 (2002)
3. G. Blasse, B.C. Grabmaier, *Luminescent Materials* (Springer, Berlin, 1994)
4. C.L. Melcher, M. Schmand, M. Eriksson, IEEE Trans. Nucl. Sci. **47**, 96 (1992)
5. C.L. Melcher, J.S. Schweitzer, IEEE Trans. Nucl. Sci. **39**, 502 (1992)
6. C.L. Melcher, J.S. Schweitzer, Nucl. Instrum. Methods Phys. Res. A **314**, 212 (1992)
7. P. Dorenbos, J.T.M. de Haas, C.W.E. van Eijk, IEEE Trans. Nucl. Sci. **NS-42**(6), 2190 (1995)
8. S. David, C. Michail, I. Valais, D. Nikolopoulos, P. Liaparinos, N. Kalivas, I. Kalatzis, A. Toutountzis, N. Efthimiou, G. Loudos, I. Sianoudis, D. Cavouras, N. Dimitropoulos, C.D. Nomicos, I. Kandarakis, G.S. Panayiotakis, Nucl. Instrum. Methods Phys. Res. A **571**, 346 (2007)
9. C. Michail, S. David, P. Liaparinos, I. Valais, D. Nikolopoulos, N. Kalivas, A. Toutountzis, D. Cavouras, I. Kandarakis, G. Panayiotakis, Nucl. Instrum. Methods Phys. Res. A **580**, 558 (2007)
10. P. Liaparinos, I. Kandarakis, D. Cavouras, H. Delis, G.S. Panayiotakis, Med. Phys. **34**, 1724 (2007)
11. G.W. Ludwig, J. Electrochem. Soc. **118**, 1152 (1971)
12. R.K. Swank, Appl. Opt. **12**, 1865 (1973)
13. I. Kandarakis, D. Cavouras, G.S. Panayiotakis, C.D. Nomicos, Appl. Phys. B **72**, 877 (2001)
14. J.C. Dainty, R. Shaw, *Image Science* (Academic, New York, 1974), pp. 232–380
15. N. Kalivas, E. Costaridou, I. Kandarakis, D. Cavouras, C.D. Nomicos, G.S. Panayiotakis, Nucl. Instrum. Methods Phys. Res. A **490**, 614 (2002)
16. G. Borasi, A. Nitrosi, P. Ferrari, D. Tassoni, Med. Phys. **30**, 1719 (2003)
17. E. Samei, M.J. Flynn, Med. Phys. **29**, 447 (2002)
18. G.E. Giakoumakis, Appl. Phys. A **52**, 7 (1991)
19. I. Kandarakis, D. Cavouras, C.D. Nomicos, G.S. Panayiotakis, Appl. Phys. B **68**, 1121 (1999)
20. R.M. Nishikawa, M.J. Yaffe, Med. Phys. **17**, 894 (1990)
21. J. Lindstrom, G.A. Carlsson, Phys. Med. Biol. **44**, 1353 (1999)
22. I. Kandarakis, D. Cavouras, G.S. Panayiotakis, C.D. Nomicos, Phys. Med. Biol. **42**, 1351 (1997)
23. D. Cavouras, I. Kandarakis, D. Nikolopoulos, I. Kalatzis, G. Kagadis, N. Kalivas, A. Episkopakis, D. Linardatos, M. Roussou, E. Nirgianaki, D. Margetis, I. Valais, I. Sianoudis, K. Kourkoutas, N. Dimitropoulos, A. Louizi, C. Nomikos, G. Panayiotakis, Appl. Phys. B **80**, 923 (2005)
24. J.M. Boone, in *Handbook of Medical Imaging*. Physics and Psychophysics, vol. 1 (SPIE, Bellingham, 2000)
25. J.R. Greening, *Fundamentals of Radiation Dosimetry* (Institute of Physics, London, 1985)
26. G.T. Barnes, *The Physics of Medical Imaging: Recording System Measurements and Techniques* (Am. Assoc. Phys. Med., New York, 1979)
27. ICRU Rep. 41 (1986)
28. D. Cavouras, I. Kandarakis, T. Maris, G.S. Panayiotakis, C.D. Nomicos, Appl. Phys. A **72**, 67 (2001)
29. A.L. Evans, *The Evaluation of Medical Images* (Hilger, Bristol, 1981)
30. J.C. Blakesley, R. Speller, Med. Phys. **35**(1), 225 (2008)